

New Planetary Nebulae in the Galactic bulge region with $l > 0^\circ$ - II.

P. Boumis^{1*}, S. Akras^{1,2}, E. M. Xilouris¹, F. Mavromatakis³, E. Kapakos²,
J. Papamastorakis^{2,4}, and C. D. Goudis^{1,5}

¹*Institute of Astronomy & Astrophysics, National Observatory of Athens, I. Metaxa & V. Paulou, GR-152 36 P. Penteli, Athens, Greece.*

²*Department of Physics, University of Crete, P.O. Box 2208, GR-710 03 Heraklion, Crete, Greece.*

³*Technological Education Institute of Crete, General Department of Applied Science, P.O. Box 1939, GR-710 04 Heraklion, Crete, Greece.*

⁴*Foundation for Research and Technology-Hellas, P.O. Box 1527, GR-711 10 Heraklion, Crete, Greece.*

⁵*Astronomical Laboratory, Department of Physics, University of Patras, GR-265 00 Rio-Patras, Greece.*

Accepted 2006 January 9; Received 2005 December 28; in original form 2005 July 27

ABSTRACT

The presentation of new results from an [O III] 5007 Å survey in a search for planetary nebulae (PNe) in the galactic bulge is continued. A total of 60 objects, including 19 new PNe, have been detected in the remaining 34 per cent of the survey area, while 41 objects are already known. Deep H α + [N II] CCD images as well as low resolution spectra have been acquired for these objects. Their spectral signatures suggest that the detected emission originates from photoionized nebulae. In addition, absolute line fluxes have been measured and the electron densities are given. Accurate optical positions and optical diameters are also determined.

Key words: surveys – planetary nebulae: general - Galaxy: bulge.

1 INTRODUCTION

This is the second of a series of papers presenting optical imaging and spectrophotometric results on newly discovered planetary nebulae. In Paper I (Boumis et al. 2003), the discovery method and first results on the [O III] 5007 Å survey, in the northern Galactic bulge, were presented.

PNe are powerful tracers of our Galaxy’s star formation history (Paper I; Beaulieu et al. 2000 and references therein). The study of PNe can provide insight to the late stages of stellar evolution, the nucleosynthesis in low and intermediate mass stars (1 M $_{\odot}$ to 8 M $_{\odot}$) and the chemical evolution of galaxies. When a low or intermediate mass star is closing to its end, it goes through the red-giant (RG) phase, followed by a heavy mass-loss period known as the asymptotic-giant-branch (AGB) stage. Finally, it becomes a white-dwarf (WD) surrounded by a planetary nebula (PN) made up of ionized gas from earlier stages of mass-loss.

PNe near the Galactic center can be considered to lie, roughly, at the same distance. Approximately 500 PNe have been discovered up to now, while \sim 3500 have been discovered in our Galaxy (Paper I and references therein; Parker et al. 2003, 2005a,b; Jacoby & van de Steene 2004). These numbers are considered small when compared with that generally expected (15000 to 30000; Acker et al. 1992a; Zijlstra & Pottasch 1991). Therefore, our Galaxy and especially, the Bulge area is well suited to search for new PNe.

Information concerning the [O III] survey (observations and analysis) are given in sect. 2, while in sect. 3 the follow-up observations are presented (CCD imaging and spectroscopy) of the newly discovered PNe. In addition, flux measurements, diameter determination, accurate positions and other physical properties for the new PNe are given in sect. 4. In an forthcoming paper (Paper III – in preparation), we will present photoionization modelling applied to the new PNe, in order to gain more insight into their physical parameters. In particular, flux calibrated images for most of the new PNe together with their spectroscopic results will be used in a PNe photoionization model (CLOUDY; e.g. van Hoof & van de Steene 1999).

2 THE [O III] 5007 Å SURVEY

2.1 Observations & Results

The observations were performed with the 0.3 m Schmidt-Cassegrain (f/3.2) telescope at Skinakas Observatory in Crete, Greece in June 14–23 & 26–28 and July 16–20, 2001. An [O III] 5007 Å interference filter with an 28 Å bandwidth was used in combination with a Thomson CCD (1024 \times 1024). This configuration results in a scale of 4.12 arcsec pixel⁻¹ and a field of view of 71 \times 71 arcmin² on the sky. In our survey we observed the regions $10^\circ < l < 20^\circ$, $-10^\circ < b < -3^\circ$ and $0^\circ < l < 20^\circ$, $3^\circ < b < 10^\circ$ (Fields A and B in Fig. 1 - total coverage on sky \sim 220 square degrees). The filled dark rectangles in Fig. 1 represent the observed fields. The remaining region of 34 per cent of

* e-mail: ptb@astro.noa.gr

the proposed grid (63 fields out of 179) is covered, which was not observed because of the availability of the telescope. All targets were observed between airmass 1.4 to 2.0 in similar observing and seeing (1 – 2 arcsec) conditions.

Two exposures in [O III] 5007 Å of 1200 s and three exposures in the continuum, each of 180 s, were obtained to identify and remove any cosmic ray hits. Two different continuum filters were used, depending on their availability. Details about the filters, the selection criteria and the detection method are given in Paper I. After a detailed and systematic visual investigation of the remaining 63 fields, 60 objects were identified. Images outlining the analysis procedure through the various steps can be found in Paper I.

After identifying the PNe candidates, a preliminary astrometry solution was obtained for all images containing one or more candidates (see Paper I for details). Sixty (60) objects were detected in these images. In order to identify the already known PNe, we used up-to-date published catalogues related to planetary nebulae (see Table 3 in Paper I). The search showed that among the objects found in our survey, 41 of them are known PNe, while 19 objects are new PNe candidates. Note that independent work by Parker et al. (2003, 2005b) resulted in a new catalogue of PNe, where 9 of our new PNe candidates are included as new or candidate PNe (see Table 1).

As in Paper I, a search in the IRAS Point Source Catalog (1988) was performed for the presence of dust at the positions of the new PNe candidates. The correlation revealed 4 matches (see Table 1). Taking into account their low flux quality density, a reasonable number of them satisfy the standard criteria ($F_{12}/F_{25} \leq 0.35$ and $F_{25}/F_{60} \geq 0.3$ – Pottasch et al. 1988; van de Steene 1995) used to consider a new object as a probable PN. A cross-check of our new PNe list was also performed with the 2MASS Point Source Catalog (2000), the MSX infrared astrometric Catalog (Egan et al. 1999) and the radio known PNe catalog. However, the results were negative and it may be that the low sensitivity of these surveys prevented a positive identification. In a very recent paper, Luo et al. (2005) presented radio identifications for 315 recently discovered PNe using the 1400 MHz (NVSS) images. Since the radio catalogue was just published, all our new PNe (including those of Paper I) were examined. A detailed check of this catalogue showed that there is a possibility of correlation between the radio sources and a number of our new PNe. Following Luo et al. (2005), if the offset between the optical and the radio position is less than 20'', the radio source is probably identified with a PN, while offsets less than 10'' are considered positive identifications. Therefore, 15 of our new PNe were identified with radio sources. In Table 2, we present the coordinates of the radio sources (Luo et al. 2005) which probably correlate with our PNe, their measured radio flux and the difference in arcseconds between the optical and the radio centres.

3 THE 1.3 METER TELESCOPE OBSERVATIONS

3.1 Imaging

Optical images of the new PNe candidates were also obtained with the 1.3 m (f/7.7) Ritchey-Cretien telescope at Skinakas Observatory during 2002 in May 19–21, June 10–14 using an H α + [N II] interference filter (75Å bandwidth). The detector was a 1024×1024 SITe CCD with a field of view of 8.5 × 8.5 arcmin². One exposure in the H α + [N II] filter of 1800 s and two exposures in the continuum, each of 180 s, were taken. All new PNe candidates observed with the H α + [N II] filter can be seen in Fig. 2. Note that they are at

the centre of each image and an arrow points to their exact position. The image size is 150 arcsec on both sides. North is to the top and east to the left. The follow-up observations were performed in the H α + [N II] filter to study the morphology of the PNe candidates and measure their angular extent.

Following the identification of the PNe candidates, an astrometric solution in all images was performed using the method presented in Paper I. Thus, the coordinates of the PNe candidates were calculated with improved accuracy. The typical rms error in the astrometric solutions was found to be ~ 0.3 arcsec. Note that the PN positional estimates are expected to be accurate to 0.5 to 1.0 arcsec. The coordinates of all new PNe candidates are given in Table 1.

3.2 Spectroscopy

Low dispersion spectra were acquired with the 1.3 m telescope at Skinakas Observatory during 2002 in June 24–28, July 16–17, 23–25 and August 12, 20–25. A 1300 line mm⁻¹ grating was used in conjunction with a 2000×800 SITe CCD covering wavelengths from 4750Å to 6815Å. This range was selected in order to observe simultaneously the H β , the H α and the sulphur lines in a single spectrum with acceptable resolution. Unfortunately, this hardware configuration does not allow the coverage of a wider range of wavelengths as well as the velocity determination. The slit width was 7.7 arcsec and it was always oriented in the south–north direction. Note that the ~ 1 Å/pxel and the dispersion of 1300 line mm⁻¹ result in a resolution of ~ 8 Å and ~ 11 Å in the red and blue wavelengths, respectively. The exposure time of the individual spectra ranges from 3600 to 3900 s depending on the observing window of each object. The spectrophotometric standard stars HR5501, HR7596, HR9087, HR718, and HR7950 (Hamuy et al. 1992) were observed for the absolute calibration of the spectra. The low resolution spectra were taken on the relatively bright optical part of each PN candidate. The actual spectra can be seen in Fig. 3, while in Table 3 the line fluxes, corrected for interstellar reddening, are given. The interstellar extinction $c(H\beta)$ and observational reddening E_{B-V} were derived using the equations presented in Paper I. Due to the high interstellar extinction in the direction of the bulge, a second estimation of E_{B-V} was made using the SFD code (Schlegel, Finkbeiner & Davis 1998). The comparison shows a general agreement between the two E_{B-V} calculations within a 3 σ error. The signal to noise ratios do not include calibration errors, which, typically, are less than 10 percent. The absolute H α fluxes (in units of 10⁻¹⁶ erg s⁻¹ cm⁻² arcsec⁻²), the exposure time of each individual spectra, the interstellar extinction $c(H\beta)$ with its estimated error and the reddening E_{B-V} (resulting from our observations and SFD maps) are listed in Table 4.

4 DISCUSSION

The H α + [N II] images as well as the low resolution spectra of the newly discovered PNe candidates were used for a more detailed study. In Fig. 4(a), the IRAS colour–colour diagram is plotted for 13 of our objects (including these of Paper I) overlaid on the corresponding colour–colour plot of known PNe (Acker et al. 1992b), for comparison reasons. The known PNe used in this diagram possess good flux quality (filled circles) and poor quality (open rectangles). It seems that the new objects belong, or are close, to the region of PNe according to the criteria presented in Sect. 2.1. In addition, the diagnostic diagram of $\log(H\alpha/[N II])$ vs. $\log(H\alpha/[S II])$ of Garcia et al. (1991), together with our measured relative line fluxes

Table 1. Newly discovered PNe.

Object	PN G (III.1 ± bb.b)	RA (J2000)	Dec (J2000)	IRAS source	F ₁₂ (Jy)	F ₂₅ (Jy)	F ₆₀ (Jy)	F ₁₀₀ (Jy)	F _{Quality} (12,25,60,100 μm)	Ref ^a
PTB26	008.3+09.6	17 29 13.1	-16 47 42.6							1b
PTB27	008.4-02.8	18 15 12.7	-23 01 03.8							2a
PTB28	008.6+06.7	17 40 21.1	-18 05 08.9	17374-1803	4.71	2.97	0.51	4.32	3,3,1,1	
PTB29	008.7-04.2	18 21 08.2	-23 23 56.9							2a
PTB30	010.1+04.4	17 51 46.6	-18 04 05.0							1a
PTB31	011.0-02.9	18 20 53.7	-20 48 10.9	18179-2049	0.36	0.67	3.1	88.6	1,3,3,1	1b
PTB32	011.3-09.1	18 45 10.2	-23 21 39.7							
PTB33	011.4-05.3	18 30 41.9	-21 31 51.0							2b
PTB34	011.8-05.0	18 30 07.7	-21 05 02.6							
PTB35	012.1-02.6	18 21 43.7	-19 39 45.7							1a
PTB36	013.2-05.0	18 32 45.3	-19 49 32.2							1a
PTB37	013.7-04.7	18 32 34.6	-19 14 03.7							1a
PTB38	013.8-02.0	18 23 04.3	-17 53 31.5	18201-1755	1.58	1.05	22.4	258	1,3,1,1	
PTB39	014.2-03.4	18 29 00.2	-18 10 46.2							
PTB40	014.3-07.2	18 43 39.6	-19 48 30.9							
PTB41	014.8-02.7	18 27 26.6	-17 24 10.0							
PTB42	015.3-03.3	18 30 22.9	-17 11 53.7							
PTB43	016.6-04.0	18 35 55.8	-16 21 20.5	18330-1623	1.14	1.46	4.4	68.8	3,3,1,1	
PTB44	016.9-09.7	18 57 39.8	-18 36 16.0							

^a Independently discovered by Parker et al. (2003, 2005b) as new PNe (1a, 2a) and candidate PNe (1b, 2b).

Table 2. Radio sources (Luo et al. 2005) which probably are correlated with the new PNe. Note that radio identification for the PNe of Paper I can also be seen.

Object	RA ^a (J2000)	Dec ^a (J2000)	S _{1.4GHz} (mJy)	difference ^b (arcsec)
PTB01	17 43 38.88	-24 31 58.2	4.3	6.81
PTB05	17 41 38.97	-21 44 33.9	4.5	4.19
PTB11	18 13 40.63	-23 57 38.0	2.7	5.93
PTB12	17 47 15.74	-19 57 23.3	2.3	4.76
PTB13	17 51 07.74	-19 25 40.8	3.0	14.8
PTB15	17 57 5.85	-17 11 05.5	2.2	5.51
PTB17	17 57 10.61	-15 56 20.5	3.7	3.55
PTB19	17 58 26.35	-14 25 22.6	8.5	5.66
PTB20	17 52 14.97	-11 10 37.6	7.6	2.05
PTB23	18 31 51.05	-14 15 19.6	10.9	10.3
PTB25	18 32 04.70	-13 26 16.3	5.9	3.86
PTB26	17 29 12.73	-16 47 45.7	2.4	6.20
PTB27	18 15 13.07	-23 01 05.2	3.2	13.5
PTB30	17 51 44.84	-18 04 25.5	3.8	32.5
PTB31	18 20 53.71	-20 48 13.6	15.0	2.74
PTB32	18 45 11.09	-23 21 21.7	2.9	21.7
PTB34	18 30 08.17	-21 05 10.1	3.6	10.0
PTB35	18 21 43.32	-19 39 44.5	2.5	5.52
PTB38	18 23 04.51	-17 53 36.2	10.1	5.52

^a RA, Dec of the radio source.

^b Difference between the optical and the radio centre.

confirm the photoionization origin (Fig. 4(b)) of the candidate PNe. The [S II]/H α ratios are in all cases less than 0.3. Nine of them display very low S/N ratio in their [N II] and [S II] emission lines and are not presented in Table 3. However, their [S II]/H α is less than 0.2.

The angular diameters of the new PNe candidates have been measured in the H α + [N II] images acquired with the 1.3 m tele-

scope and were established with the method described below. This method was applied because, especially for the faint PNe, it was difficult to accurately calculate the diameters because their outer areas were below the 3 σ level in the original images. In the case of elliptical shells, the major and the minor axes are given. The method used to determine the angular diameters involves the conversion of their intensity values in a scale ranging from 0 to 1000.

In particular, for intensities higher than 85% of the maximum, a value of 1000 was assigned, while for values between 65% to 85%, 50% to 65%, 35% to 50%, 20% to 35%, 10% to 20% and below 10% of the maximum intensity, values of 800, 600, 400, 200, 50, 25 were given. The advantage of this transformation is that having this wide range of values, the intensity of the object can be distinguished from the sky background with much better accuracy, and consequently, their outer part can be clearly determined. For PNe with well defined outer edges (i.e. with a steep drop-off of the surface brightness), it was easy to measure the diameter using either the original $H\alpha + [N II]$ image or the above method. However, in case of faint PNe the direct use of the images results in larger errors compared to this method. This was also demonstrated by Ruffe et al. (2004) (and references therein) who showed that the flux drops very fast between intensity levels in the interval of 15 to 5 per cent of the peak surface brightness and therefore, it is hard to determine the actual boundary of the PN. In our case, values between 10 to 20 per cent of the peak surface brightness contour were selected in order to measure the diameter of each object and in all cases the estimated numbers are greater than the 3σ limit. An example of the method is shown in Fig. 5, where an enlargement of the original $H\alpha + [N II]$ image of PTB34 can be seen in Fig.5(a). The image of the same PN is shown in Fig.5(b), which is derived by applying the method described above. The angular diameter was measured in both images but the results from the second image were more accurate. The resulting images were also used to determine the morphological type of each PN. All dimensions are given in Table 4. Thirteen of the new PNe are characterized by diameters less than 20 arcsec (Bulge limit – Gathier et al. 1983), three are close to this limit, and three by diameters greater than 30 arcsec. The possibility that the latter are more evolved and/or are nearby cannot be excluded.

The distribution of the new PNe (a) in galactic latitude and (b) in angular diameter shows a strong concentration towards the bulge and especially, when $-6^\circ < b < 6^\circ$ and between 4 to 20 arcsec. Both results are in agreement with what is expected for PNe in the Galactic bulge. Note that due to the high interstellar extinction no observations were performed in the range $-3^\circ < b < 3^\circ$, while, due to the limited resolution of the survey observations, objects with diameters smaller than 4 arcsec could not be identified.

A morphological type was assigned to the new PNe (Table 4) according to the classification of Manchado et al. (2000). Approximately, 28 percent of the new PNe display spherical, well-defined shells, 42 percent appear elliptical and the rest are bipolar or unclear. The different morphological PNe classes seen in our survey can be found in Boumis & Bryce (2004). Objects like PTB34, PTB36 display a ring-like structure, while for example, PTB26, PTB32 possess incomplete bright shells. Bright compact nebulae like PTB28, PTB38, PTB42, PTB43 are also detected. However, their morphological type cannot be resolved clearly with the current data. Moreover, the morphological class of some PNe could not be determined unambiguously and even though, these have been classified as round, the possibility that they are elliptical cannot be ruled out. The electron densities were found to be different for each morphological class. The median value for ellipticals is higher than that for round and bipolar PNe. Also, at a first glance the $[N II]/H\alpha$ and N/O ratios are higher for round than for elliptical PNe. The morphology of PNe provides the opportunity to obtain a better understanding of the evolution of stars. It is generally accepted that the different PNe morphologies are attributed to progenitors of different masses. According to Phillips (2003) (and references therein), circular PNe arise from stars with low mass progenitors, the bipo-

lar arise from higher mass stars, while elliptical originate from a range of masses of the progenitors. Furthermore, the morphological differences can also be attributed to the PN stage of evolution. Compact nebulae in their first stages of expansion appear stellar and relatively bright, while large nebulae with faint surface brightness are in their late evolutionary stage.

Following the procedure described in Paper I and assuming a temperature of 10^4 K (Cuisinier et al. 2000), an estimation of the electron density $n_{[S II]}$ was made, with the “temden” task of the “nebular” package in IRAF, for each specific Sulfur line ratio ($[S II] 6716\text{\AA}/[S II] 6731\text{\AA}$). The electron densities and their associated errors are given in Table 4. In addition, using the observed $[N II] 6548 + 6584\text{\AA}/[N II] 5755\text{\AA}$ ratios, an estimate of the electron temperature $T_{[N II]}$ was made, whenever possible. In fact, only for three of our new PNe temperatures close to 10000 K were found. The high interstellar extinction towards the Galactic bulge as well as the low surface brightness for many of the new PNe prevented the registration of high quality spectra. This affects mainly the lower intensity lines like $[S II]$ or $He II 5411$ & 6234 Å, which are faint or even undetectable. For all the PNe candidates in our survey, $H\alpha$, $[O III]$ and $H\beta$ emission lines could be measured and in most cases, $[N II] 6548$ & 6584 Å. However, the spectra of some of the new PNe (e.g. PTB36) have a low signal to noise and only $H\beta$, $H\alpha$ and $[O III]$ are well determined. Since these PNe are found in a region of significant extinction shorter wavelengths are more affected than longer wavelengths.

In Table 3 we list the fluxes, measured in our long-slit spectra, corrected for interstellar extinction, where it is evident that almost all PNe display very strong $[O III] 5007$ Å emission relative to $H\alpha$. It is known that the N/O and He abundances reflect the mass distribution of the progenitor star, with more massive objects having higher N/O and He abundances in comparison with the low-mass objects (Cuisinier et al. 2000). In our case, the abundances in N/O and He are generally low implying old progenitor stars. The latter suggests that they belong to the Galactic bulge region according to Webster (1988) and Cuisinier et al. (2000). Both authors showed that the Galactic bulge PNe originate from old progenitors with low N/O and He abundances. The excitation classes of our new PNe were studied according to the classification criteria of Aller (1956), Feast (1968) and Webster (1975). They are derived basically from the ratios of $[O III]/H\beta$, $He II 4686\text{\AA}/H\beta$, $[O II] 3727\text{\AA}/[O III] 4959\text{\AA}$ and $He II 4686\text{\AA}/He I 5876\text{\AA}$. In our case, following the relation 2.1a of Dopita & Meatheringham (1990), the $[O III]/H\beta$ ratio suggests that our new PNe belong to the low (2–4) and medium (4–6) excitation classes. It is only PTB42 showing an excitation class greater than 6 and therefore, it must be highly ionized. However, the $He II 4686$ Å and $[O II] 3727$ Å emission lines are outside the observed range due to the hardware configuration (see Sect. 3.2) and thus, it is not possible to better confine the actual excitation class of each PN.

5 CONCLUSIONS

We presented results from the narrow band $[O III] 5007$ Å survey of PNe in the Galactic bulge ($l > 0^\circ$). Covering the remaining 34 percent of our selected region, we detected 60 objects, including 41 known PNe and 19 new PNe. $H\alpha + [N II]$ images as well as low resolution spectra of the new PNe were taken which confirmed the photoionized nature of the emission. About 84 percent of the detected objects have angular sizes ≤ 20 –25 arcsec, while all show $H\alpha/[O III] 5007$ Å ratios less than 1. Four (4) of our new PNe are

Table 3. Line fluxes.

Line (Å)	PTB26	PTB27	PTB28	PTB29	PTB30	PTB31	PTB32
H β 4861	100 (45) ^a	100 (21)	100 (26)	100 (21)	100 (14)	100 (25)	100 (15)
[O III] 4959	49 (33)	330 (42)	312 (52)	233 (37)	252 (24)	203 (40)	159 (26)
[O III] 5007	154 (54)	926 (78)	864 (90)	725 (70)	770 (43)	601 (73)	455 (65)
HeII 5411	–	–	–	–	–	–	–
[N I] 5200	–	–	16 (11)	–	–	–	–
[N II] 5755	–	–	4 (4)	–	–	–	–
HeI 5876	15 (26)	–	15 (14)	11 (10)	–	14 (15)	15 (7)
HeII 6234	–	–	–	–	–	–	–
[O I] 6300	–	4 (12)	32 (34)	–	–	–	–
[S III] 6312	–	–	8 (10)	–	–	–	–
[O I] 6363	–	–	8 (11)	–	–	–	–
[Ar V] 6435	–	–	–	–	–	–	–
[N II] 6548	34 (50)	5 (20)	65 (42)	20 (14)	–	5 (17)	79 (43)
H α 6563	285 (147)	285 (129)	285 (98)	285 (84)	285 (60)	285 (177)	285 (86)
[N II] 6584	90 (85)	12 (28)	210 (85)	65 (36)	16 (12)	12 (31)	236 (81)
HeI 6678	5 (13)	–	7 (8)	–	–	4 (15)	5 (8)
[S II] 6716	22 (34)	4 (20)	41 (27)	9 (11)	–	2 (9)	36 (27)
[S II] 6731	15 (28)	3 (18)	44 (30)	7 (9)	–	2 (7)	27 (22)
Line (Å)	PTB33	PTB34	PTB35	PTB36	PTB37	PTB38	PTB39
H β 4861	100 (11)	100 (61)	100 (26)	100 (13)	100 (16)	100 (17)	100 (35)
[O III] 4959	200 (23)	207 (100)	240 (54)	303 (33)	231 (30)	429 (65)	389 (77)
[O III] 5007	637 (44)	611 (182)	711 (100)	919 (63)	643 (57)	1242 (125)	1130 (140)
HeII 5411	–	8 (25)	–	–	–	–	–
[N I] 5200	–	–	–	–	–	–	–
[N II] 5755	–	–	–	–	–	–	–
HeI 5876	9 (5)	4 (19)	6 (14)	–	–	16 (22)	13 (29)
HeII 6234	–	–	–	–	–	–	–
[O I] 6300	–	–	7 (22)	–	–	5 (12)	–
[S III] 6312	–	2 (8)	–	–	–	2 (5)	–
[O I] 6363	–	–	3 (16)	–	–	2 (3)	–
[Ar V] 6435	–	1 (7)	–	–	–	–	–
[N II] 6548	38 (16)	0.4 (8)	184 (142)	–	–	9 (32)	2 (11)
H α 6563	285 (47)	285 (250)	285 (195)	285 (76)	285 (85)	285 (225)	285 (190)
[N II] 6584	105 (28)	2 (8)	569 (255)	–	–	29 (72)	3 (16)
HeI 6678	–	2 (15)	5 (19)	–	–	3 (16)	2 (14)
[S II] 6716	30 (12)	0.8 (9)	20 (41)	–	–	3 (13)	–
[S II] 6731	27 (10)	0.6 (8)	15 (33)	–	–	6 (23)	–
Line (Å)	PTB40	PTB41	PTB42 ^a	PTB43 ^a	PTB44		
H β 4861	100 (25)	100 (24)	100 (24)	100 (45)	100 (35)		
[O III] 4959	376 (57)	212 (43)	895 (89)	238 (80)	363 (51)		
[O III] 5007	1146 (103)	609 (79)	2620 (161)	710 (147)	1085 (96)		
HeII 5411	–	9 (8)	5 (6)	–	–		
[N I] 5200	–	–	–	–	–		
[N II] 5755	–	–	44 (32)	3 (13)	–		
HeI 5876	4 (8)	–	13 (12)	19 (44)	–		
HeII 6234	–	–	–	–	–		
[O I] 6300	–	–	20 (21)	3 (18)	–		
[S III] 6312	–	–	–	5 (23)	–		
[O I] 6363	–	–	–	–	–		
[Ar V] 6435	–	–	–	–	–		
[N II] 6548	–	–	182 (83)	5 (32)	–		
H α 6563	285 (101)	285 (140)	285 (99)	285 (219)	285 (89)		
[N II] 6584	–	2 (4)	607 (147)	16 (65)	10 (8)		
HeI 6678	–	–	4 (8)	4 (25)	–		
[S II] 6716	–	–	–	1 (11)	–		
[S II] 6731	–	–	–	2 (16)	–		

^a Numbers in parentheses represent the signal to noise ratio of the line fluxes, measured at the center of the corresponding emission line profile. All fluxes are normalized to F(H β)=100 and are corrected for interstellar extinction.

Table 4. Exposure time and basic physical parameters.

Object	Exp. time ¹	Diameter ²	M.Type ³	F(H α) ⁴	c(H β) ⁵	$\sigma_{c(H\beta)}^6$	E _{B-V} ⁷ (OBS)	$\sigma_{E_{B-V}}^8$	E _{B-V} ⁹ (SFD)	n _[S II] ¹⁰	$\sigma_{n_{[S II]}}^{11}$
PTB26	3600	28.5×16.0	B	5.8	0.62	0.03	0.43	0.02	0.39	<0.07	–
PTB27	3600	12.0	R	4.7	1.86	0.10	1.29	0.07	1.45	0.36	0.15
PTB28	3600	4.5	–	4.1	0.69	0.05	0.48	0.03	0.48	0.65	0.03
PTB29	3600	37.0×34.0	E	7.4	0.92	0.04	0.64	0.03	0.66	0.16	0.03
PTB30	3600	26.0	R	2.1	1.57	0.15	1.08	0.10	0.99	–	–
PTB31	3900	15.5	R	10.7	2.72	0.14	1.88	0.10	1.91	0.67	0.33
PTB32	3600	135.0×115.0	E	1.5	0.74	0.11	0.51	0.08	0.39	<0.07	–
PTB33	3600	17.0	R	2.0	0.58	0.11	0.39	0.08	0.49	0.38	0.07
PTB34	3900	12.5	R	36.6	1.08	0.02	0.74	0.01	0.71	<0.07	–
PTB35	3900	15.0×11.5	E	16.6	1.89	0.05	1.31	0.03	1.47	<0.07	–
PTB36	3900	22.0	B	2.5	1.02	0.16	0.71	0.11	0.62	–	–
PTB37	3900	16.0×14.0	E	4.3	1.01	0.07	0.71	0.05	0.68	–	–
PTB38	3900	5.5	–	20.7	2.47	0.10	1.71	0.07	2.07	27.0	4.7
PTB39	3900	8.0×6.5	E	12.0	1.46	0.03	1.01	0.03	1.01	–	–
PTB40	3900	11.5×10.0	E	10.9	0.99	0.06	0.69	0.04	0.46	–	–
PTB41	3600	10.5×8.0	E	11.2	1.72	0.06	1.19	0.03	1.08	–	–
PTB42	3600	4.0	–	12.7	1.41	0.04	0.98	0.03	0.69	–	–
PTB43	3900	5.0	–	26.6	1.24	0.02	0.86	0.01	0.62	4.4	1.09
PTB44	3900	58.0	E	4.5	0.92	0.04	0.64	0.03	0.24	–	–

¹ Total exposure time in sec.² Optical diameters in arcsec.³ Morphological classification according to Manchado et al. (2000), where R(=round), E(=elliptical) and B(=bipolar).⁴ Absolute H α flux in units of 10^{-16} erg s⁻¹ cm⁻² arcsec⁻².⁵ Logarithmic extinction at H β (see Sect. 3.2).⁶ 1σ error on the logarithmic extinction.⁷ Observed reddening (see Sect. 3.2).⁸ Error on the observed reddening.⁹ Reddening according to the maps of Schlegel et al. (1998) (see Sect. 3.2).¹⁰ Electron density in units of 10^3 cm⁻³ (see Sect. 5).¹¹ Error on the electron density.

found to be associated with IRAS sources. Radio sources for fifteen (15) of our new PNe (including those of paper I) were identified. All new PNe display low N/O and He abundances implying old progenitor stars, which is one of the characteristics of the Galactic bulge PNe. In a forthcoming paper (paper III), the use of the photoionization model CLOYDY will provide a deeper insight to the physical parameters of the new PNe. The information presented in papers I and II, along with the results that will be obtained from the CLOUDY model will offer a valuable tool to studies of the dynamics and kinematics of the Galactic bulge.

ACKNOWLEDGMENTS

The authors would like to thank the referee Q. Parker for his comments and suggestions and for providing us the Edinburgh/AAO/Strasbourg Catalogue of Galactic Planetary Nebulae and the Macquarie/AAO/Strasbourg H α PN Catalogue. We would also like to thank A. Acker for providing us the First Supplement to the Strasbourg–ESO Catalogue of Galactic Planetary Nebulae. The help of E. Semkov, G. Paterakis, A. Kougentakis and A. Strigachev during these observations is acknowledged. Skinakas Observatory is a collaborative project of the University of Crete, the Foundation for Research and Technology–Hellas, and the Max-Planck-Institut für extraterrestrische Physik.

REFERENCES

- Acker, A., Cuisinier, F., Stenholm, B. & Terzan, A., 1992a, *A&A*, 264, 217
- Acker, A., Ochsenbein, F., Stenholm, B., Tylanda, R., Marcout, J. & Schohn, C., 1992b, in the Strasbourg–ESO Catalogue of Galactic Planetary Nebulae, Parts 1 and 2 (Strasbourg: ESO)
- Aller, L. H., 1956, *Gaseous Nebulae* (New York: Wiley)
- Beaulieu, S. F., Freeman, K. C., Kalnajs, A. J., Saha, P. & Zhao, H., 2000, *AJ*, 120, 855
- Boumis, P., Paleologou, E. V., Mavromatakis, F. & Papamastorakis, J., 2003, *MNRAS*, 339, 735 (Paper I)
- Boumis, P. & Bryce, M., 2004, in *ASP Conf. Ser. 31, Asymmetrical Planetary Nebulae III: Winds, Structure and the Thunderbird*, eds. M. Meixner, J. H. Kastner, B. Balick & N. Soker., 3, 26
- Cuisinier, F., Maciel, W. J., Köppen, J., Acker, A. & Stenholm, B., 2000, *A&A*, 353, 543
- Dopita, M. A. & Meatheringham, S. J., 1990, *ApJ*, 357, 140
- Egan, M. P., et al., 1999, in *Astrophysics with Infrared Surveys, A Prelude to SIRTf*, ed. M. D. Bica, R. M. Cutri, & B. F. Madore, *ASP Conf. Ser.*, 177, 404
- Feast M. W., 1968, *MNRAS*, 140, 345
- García-Lario, P., Manchado, A., Riera, A., Mampaso, A. & Pottasch, S. R., 1991, *A&A*, 249, 223
- Gathier, R., Pottasch, S. R., Goss, W. W. & van Gorkom, J. H., 1983, *A&A*, 128, 325
- Hamuy, M., Walker, A. R., Suntzeff, N. B., Gigoux, P., Heathcote,

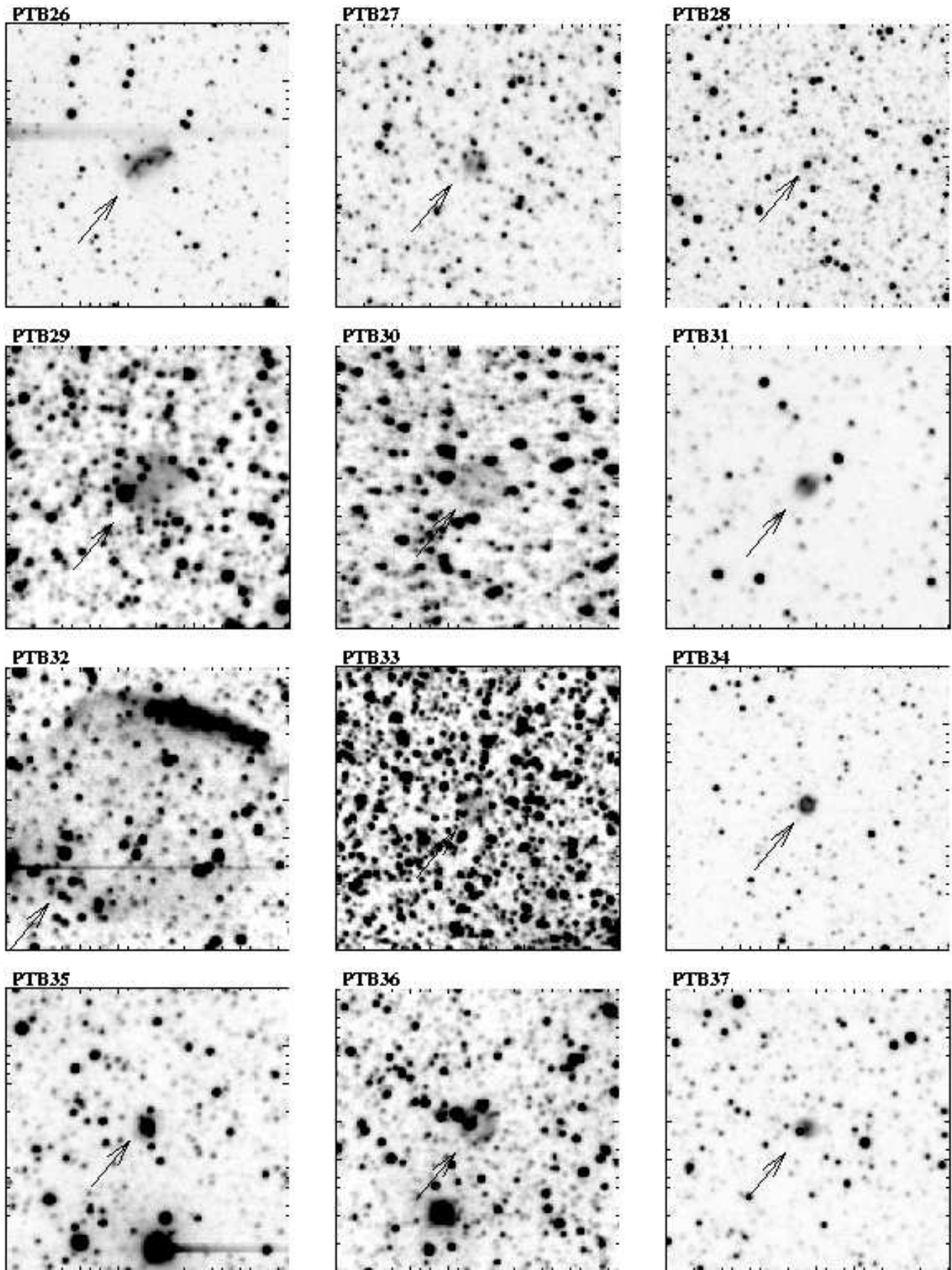


Figure 2. $H\alpha + [N II]$ images of all new PNe taken with the 1.3 m telescope. The arrows point to their position. The images have a size of $150''$ on both sides. North is at the top. East to the left.

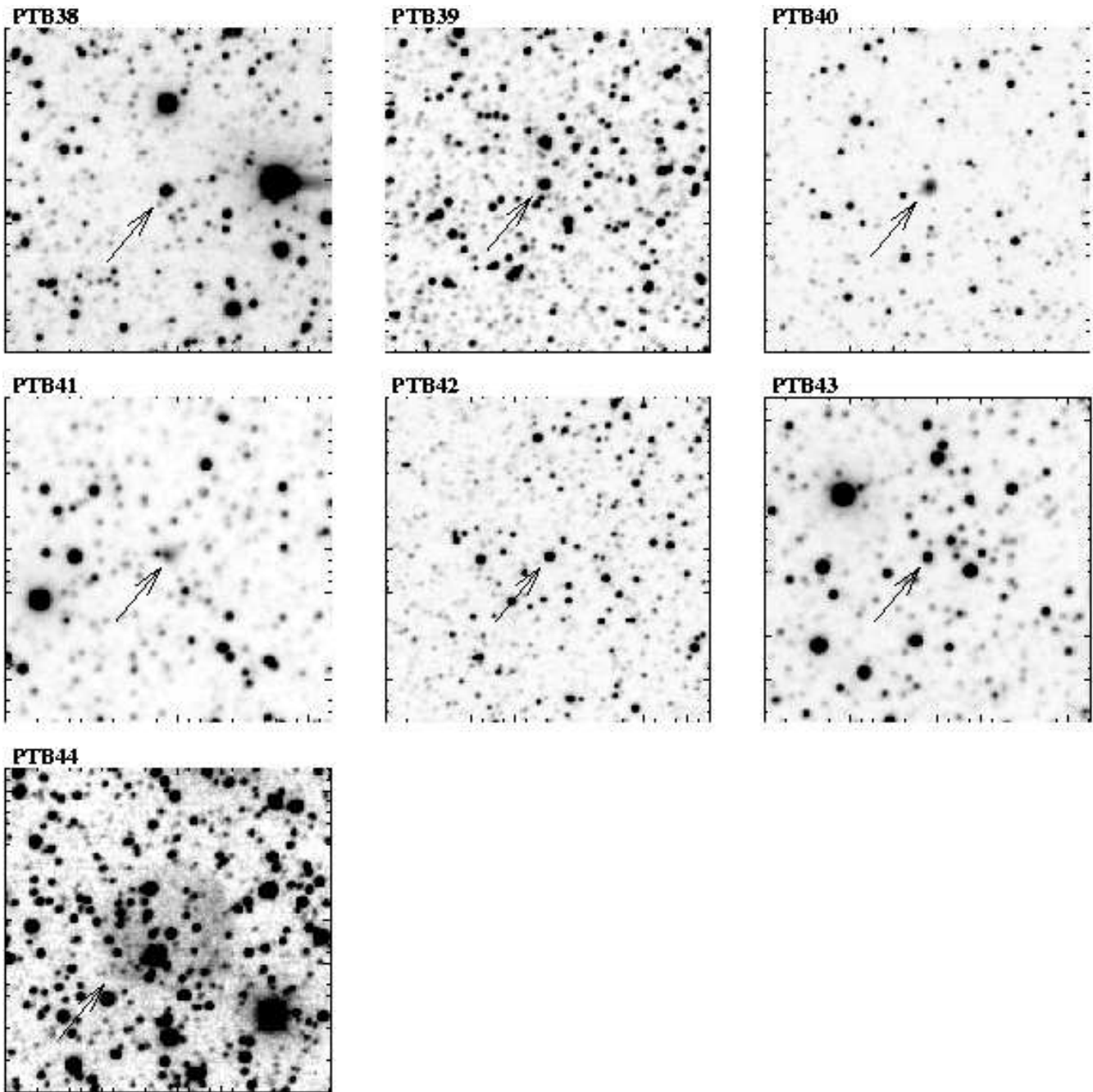
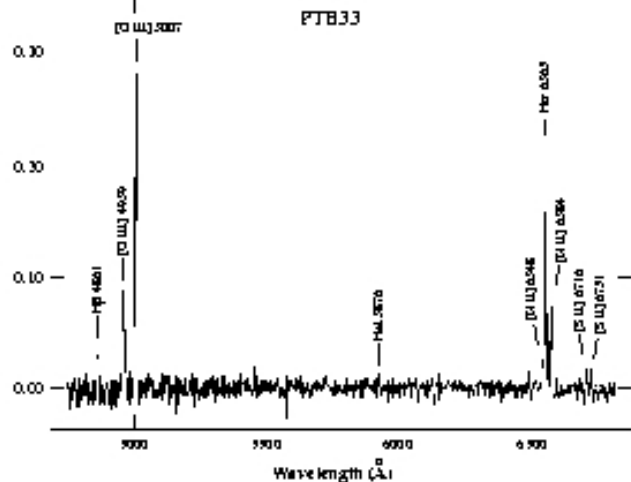
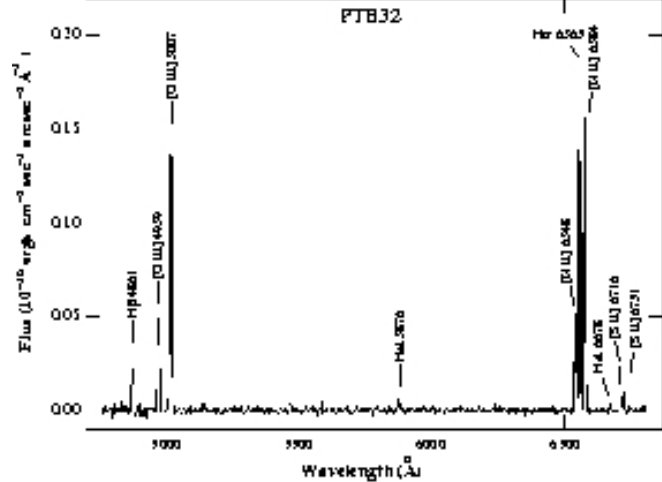
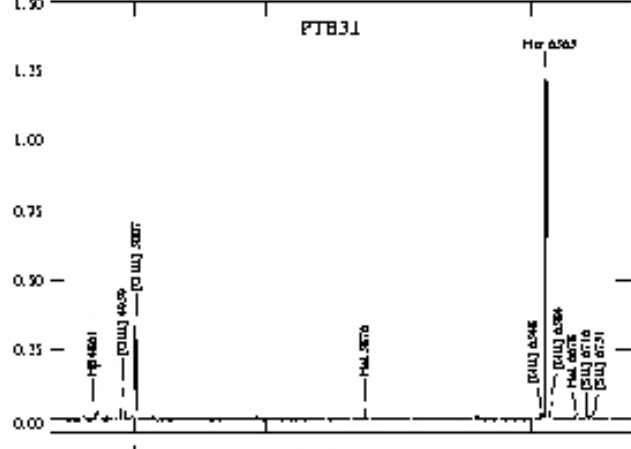
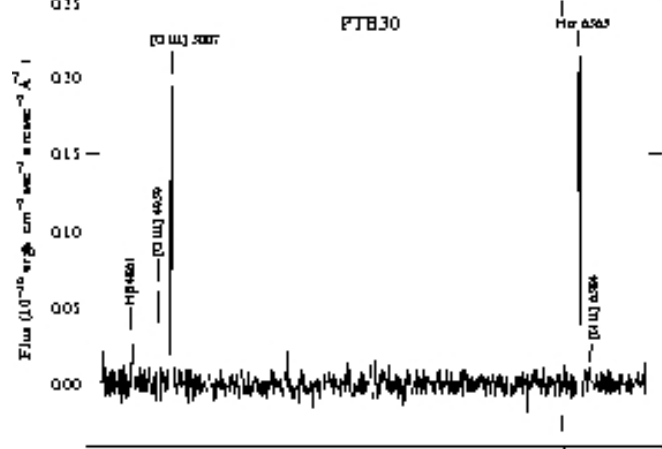
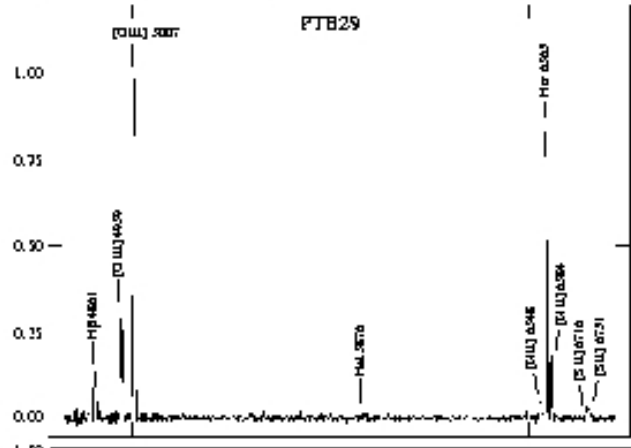
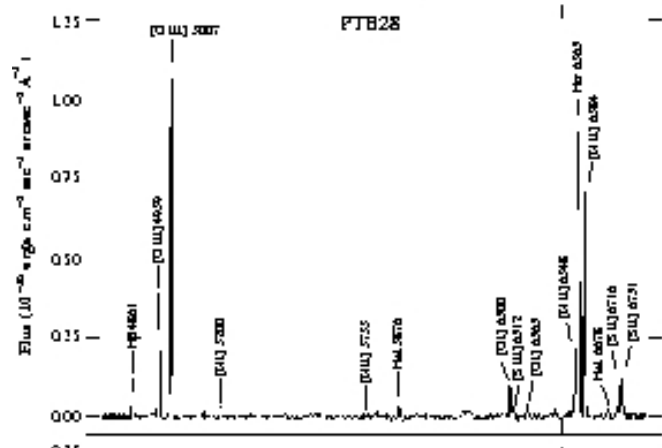
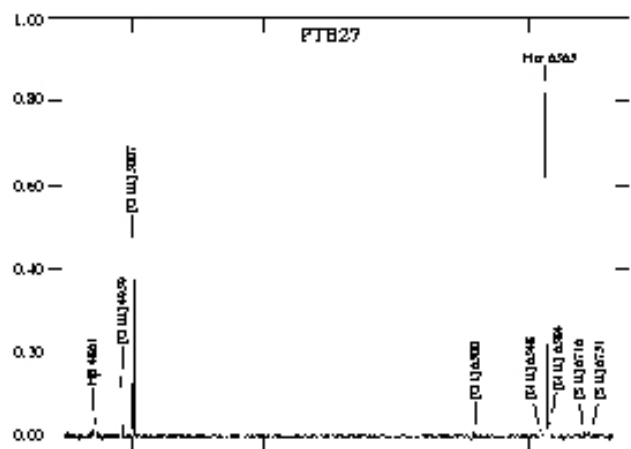
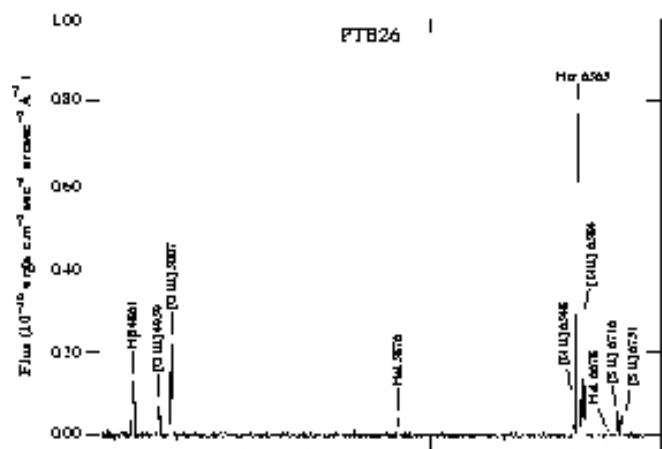


Figure 2. continued



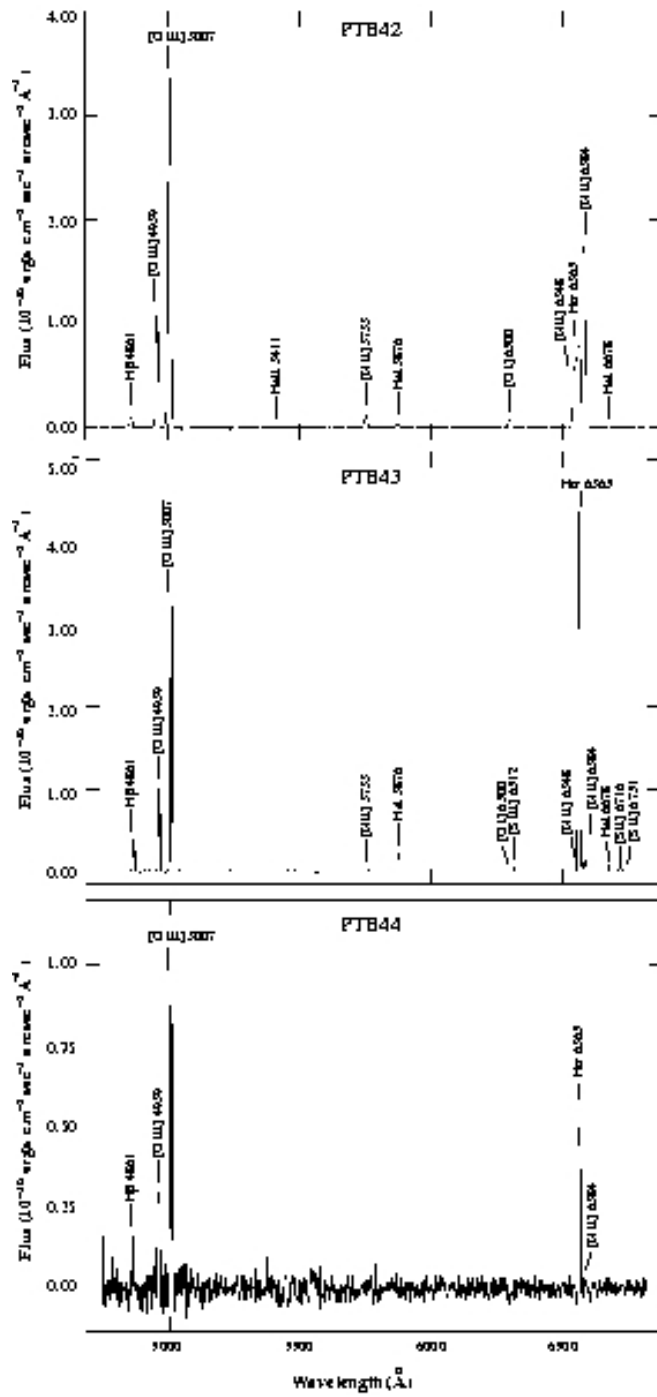


Figure 3. continued

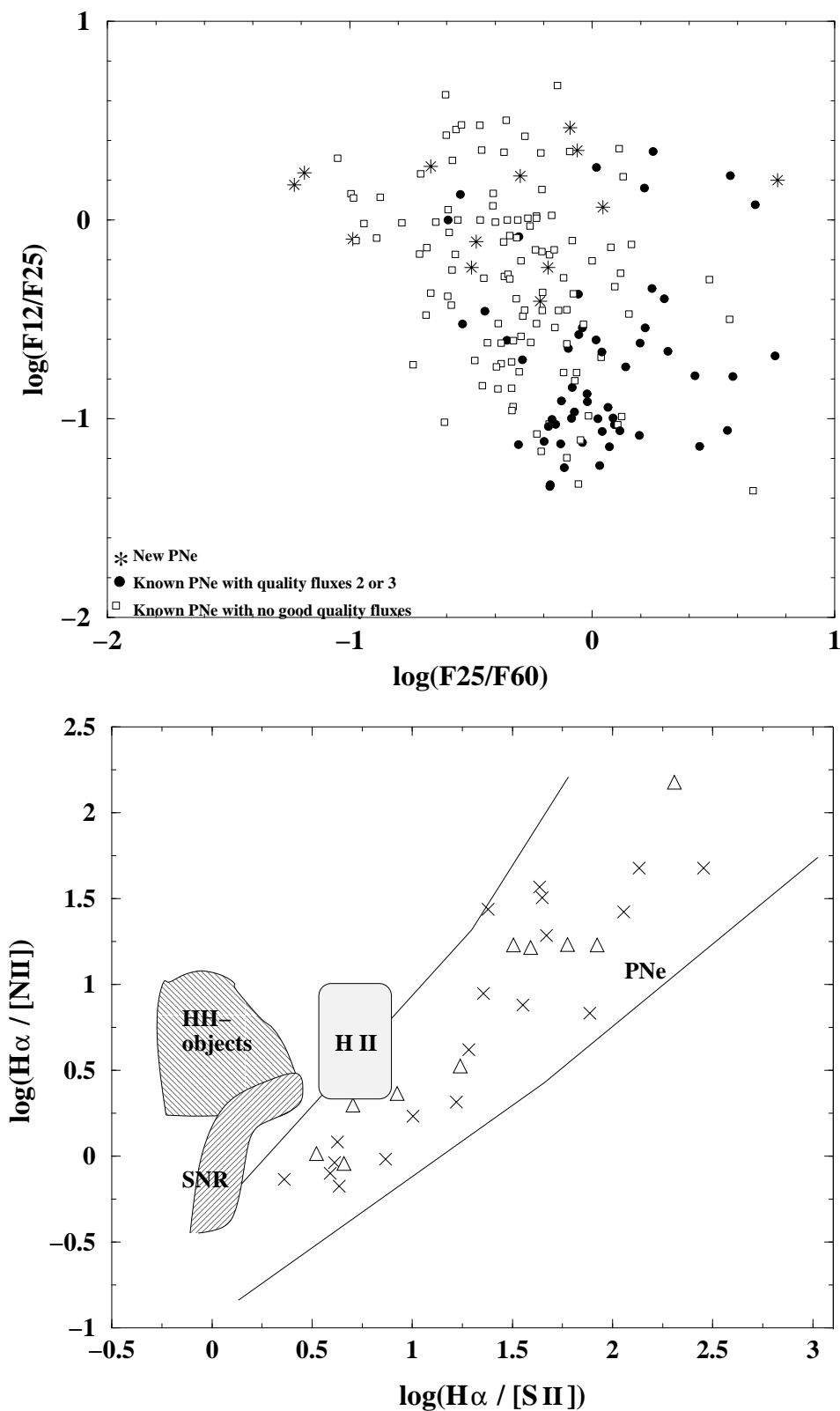


Figure 4. (a) IRAS colour–colour diagram of 13 of our objects (stars), overlaid on the colour–colour diagram of Acker’s catalogued PNe with good (circles) and not good (rectangles) quality fluxes and (b) Diagnostic diagram (Garcia et al. 1991), where the positions of the new PNe are shown with a triangle (Δ). For comparison, the position of (i) the new PNe presented in paper I are also shown with a cross (X) and (ii) other objects (supernova remnants - SNR, H II regions and Herbig Haro objects - HH) are shown, too.

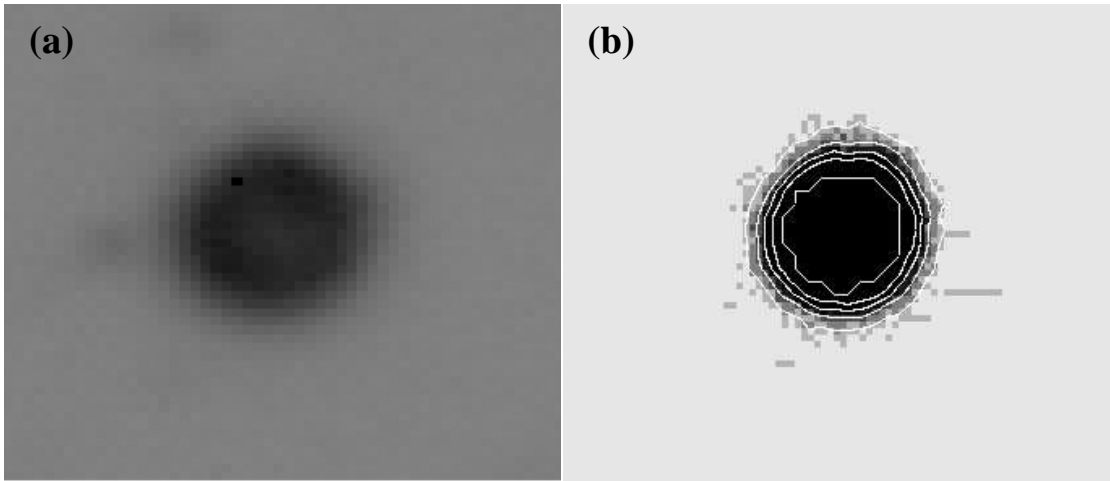


Figure 5. (a) Enlargement of the $H\alpha+[N II]$ image of PTB34 in high contrast in order to show its outer halo (b) Image of the same PN overlaid with the different scale contours as derived from the method described in the text. North is in the top, east to the left in both figures.